UNIVERSITY *of* York

This is a repository copy of *Heusler-alloy-based magnetoresistive sensor with synthetic antiferromagnet*.

White Rose Research Online URL for this paper:
https://eprints.whiterose.ac.uk/208692/

Version: Published Version

Article:

Khamtawi, R., Saenphum, N., Chantrell, R. W. orcid.org/0000-0001-5410-5615 et al. (2 more authors) (2024) Heusler-alloy-based magnetoresistive sensor with synthetic antiferromagnet. Journal of Physics D: Applied Physics. 135001. ISSN 0022-3727

https://doi.org/10.1088/1361-6463/ad1728

White Rose
university consortium
Universities of Leeds, Sheffield & York

eprints@whiterose.ac.uk
https://eprints.whiterose.ac.uk/

PAPER • OPEN ACCESS

Heusler-alloy-based magnetoresistive sensor with synthetic antiferromagnet

To cite this article: R Khamtawi *et al* 2024 *J. Phys. D: Appl. Phys.* **57** 135001

View the article online for updates and enhancements.

Heusler-alloy-based magnetoresistive sensor with synthetic antiferromagnet

R Khamtawi[1], N Saenphum[2], R W Chantrell[1,3], J Chureemart[1,3] and P Chureemart[1,3,*]

[1] Department of Physics, Mahasarakham University, Mahasarakham 44150, Thailand
[2] Seagate Technology, Teparuk, Samutprakarn 10270, Thailand
[3] School of Physics, Engineering and Technology, University of York, York YO10 5DD, United Kingdom

E-mail: phanwadee.c@msu.ac.th and pc536@york.ac.uk

CrossMark

Abstract

Heusler alloy has been widely utilized in magnetoresistive sensors to enhance the device performance. In this work, we theoretically investigate the performance of Heusler-alloy-based magnetoresistive sensors with a synthetic antiferromagnet (SAF) layer. The atomistic model combined with the spin accumulation model will be used in this work. The former is used to construct the reader stack and investigate the magnetization dynamics in the system. The latter is employed to describe the spin transport behavior at any position of the structure. We first perform simulations of the exchange bias (EB) phenomenon in the IrMn/Co$_2$FeSi (CFS) system providing a high EB field. Then, a realistic reader stack of IrMn/CFS/Ru/CFS/Ag/CFS is constructed via an atomistic model. Subsequently, the resistance–area product (RA) and magnetoresistance (MR) ratio of the reader can be calculated by using the spin accumulation model. As a result of the spin transport behavior in the Heusler-alloy-based reader stack including SAF structure at 0 K, an enhancement of the MR ratio up to 120% and RA $< 40 \, \text{m}\Omega \cdot \mu\text{m}^2$ can be observed. This study demonstrates the important role of the Heusler alloy and SAF layer in the development of magnetoresistive sensors for the application of readers in hard disk drives with an areal density beyond 2 Tb in^{-2}.

1. Introduction

Hard disk drives (HDDs) have been continually evolved to deliver a higher performance and storage capacity to meet today's requirements. The write head, read head, and recording medium are the main components, playing a prominent role in the improvement of HDD performance. Shrinking the size of the data bits is a promising way to achieve a high areal density (AD) beyond 2 Tb in^{-2} in HDDs [1–5]. A scaling down of all components in the devices is necessary, and in particular,

a reduction in the size of the read head corresponding to the size of the data bits. This subsequently results in a decrease in the performance of the read head with high thermal instability, which gives rise to noisy readback signals [6–8]. The spin valve stack is the main component of the reader, and consists of a spacer layer (SL) sandwiched by two ferromagnets (FMs). The first FM layer, regarded as a pinned layer (PL), has a fixed magnetization due to the effect of exchange bias (EB) between the FM and antiferromagnetic (AF) material, while the magnetization direction within the second FM layer or free layer (FL) can freely change depending on the induced magnetic field from the recording media. A read sensor design with a high magnetoresistance (MR) ratio, high operating speed, and reduced noise level becomes crucial for HDDs to function more efficiently. To meet this aim, choosing the appropriate materials to be utilized as the reference layer and FL is challenging.

Heusler alloys have been investigated extensively as potential materials to serve as the PL, reference layer, and FL in the reader stack [9–16]. Due to their half-metallic band structure resulting in relatively high spin polarization, they strongly enhance the efficiency of spin transport. Several studies have been reported on the characteristics of Heusler alloys used in the application of spintronic devices, such as Co_2FeSi (CFS) [12, 17–22] and $Co_2FeAlSi$ [19, 20]. Interestingly, it is seen as a promising candidate because of its high spin polarization, high saturation magnetization, and high Curie temperature. It serves more roles in the read element than only the sensing layer, leading to a high MR ratio [21, 23, 24]. Recently, CFS has been proposed as the pinned Heusler alloy layer in the EB system [25–27]. It is found that utilizing CFS as the PL can enhance the EB field and spin-polarized current.

In the conventional reader structure of AF/PL/SL/FL, the characteristics of the readback signal mainly rely on the EB field between AF and PL to fix the direction of magnetization in the PL. However, it is still insufficient to stabilize the magnetization direction of the PL. The thermal stability of the spin at the AF and FM interface is decreased as a result of the heat produced during the reading process. The spins of the AF at the interface have a tendency to stray from the easy axis, making it difficult to attain the spins of the FM to perfectly align in one direction. Thus, a synthetic AF (SAF) layer has been proposed to be added into the conventional reader stack to improve its thermal instability [28–30]. Additionally, the SAF structure is utilized to mitigate the demagnetizing field generated by the reference layer on the FL. The full reader stack, including the SAF layer, has been experimentally studied, but simulation is more complicated due to the expensive computational time.

In this work, we focus on the investigation of Heusler alloy-based current-perpendicular-to-plane giant magnetoresistance (CPP-GMR) sensors providing a high signal-to-noise ratio and low resistance–area product (RA) for the application of next-generation HDDs. In the general reader model, the effect of the diffuse interface is not taken into account, and the PL is not explicitly considered [23, 31–34]. Therefore, the atomistic model coupled with the spin accumulation model is employed here. The former allows us to construct a reader stack with diffuse interfaces at the atomistic level. For a realistic reader design, the EB system of IrMn/CFS used as the PL will also be considered by using the atomistic model. The latter is used to describe the underlying physics of the spin transport in the CPP-GMR read sensor. A realistic reader stack including the SAF layer is constructed, and the spin transport behavior is investigated through the value of the RA and MR ratio. Importantly, the AD as a function of the RA is also evaluated.

2. Methodology

To investigate the dynamics of the magnetization in the magnetic structure, the atomistic model implemented in the software package VAMPIRE [35] is used here. The time evolution of magnetization can be described by the Landau–Lifshitz–Gilbert (LLG) equation, given by

$$\frac{\partial \mathbf{S}}{\partial t} = -\frac{\gamma}{(1+\alpha^2)}(\mathbf{S} \times \mathbf{B}_{\text{eff}}) - \frac{\gamma\alpha}{(1+\alpha^2)}[\mathbf{S} \times (\mathbf{S} \times \mathbf{B}_{\text{eff}})]$$

(1)

where $\mathbf{S}$ is the normalized atomic spin vector, γ is the absolute value of the gyromagnetic ratio, and α is the intrinsic damping constant. The effective field, $\mathbf{B}_{\text{eff}}$, acting on each atomic spin can be calculated directly from the classical Hamiltonian ($\mathcal{H}$) describing the energy of the system in the Heisenberg form, given by

$$\mathcal{H} = -\sum_{i<j} J_{ij}\mathbf{S}_i \cdot \mathbf{S}_j - k_{\text{u}}\sum_i (\mathbf{S}_i \cdot \mathbf{e})^2$$
$$- \mu_{\text{s}}\sum_i \mathbf{S}_i \cdot \mathbf{B}_{\text{app}} - J_{\text{sd}}\mathbf{m} \cdot \mathbf{S}_i$$

where $\mathbf{S}_{i,j}$ is the unit vector of spin on site (i,j), J_{ij} is the nearest-neighbor exchange integral between the spin sites i and j, k_{u} is the uniaxial anisotropy constant, $\mathbf{e}$ is the unit vector of easy axis, and μ_{s} is the magnitude of the spin moment. The contributions of the exchange energy, the anisotropy energy, and the Zeeman energy are expressed in the first, second, and third terms of the spin Hamiltonian, respectively. The effect of spin torque arising from the exchange interaction between the spin accumulation ($\mathbf{m}$) and the local spin moment is included in the final term of the Hamiltonian. The effective field ($\mathbf{B}_{\text{eff}}$) acting on the spin can be determined directly by taking the first derivative of the classical Hamiltonian described above. The inclusion of the demagnetizing field and thermal fluctuations are taken into account in the model separately. The macro-cell approach is employed to consider the demagnetizing field, and the effect of finite temperature is represented as the random thermal field.

The inclusion of the demagnetizing field in $\mathbf{B}_{\text{eff}}$ can be performed by using a micro-cell approach. Using this method, the structure is discretized into cubic macrocells with uniform magnetization, and the dipolar field of the spin in the macro-cell k is calculated as follows:

$$\mathbf{B}_{\text{dip},k} = \frac{\mu_0}{4\pi}\sum_{l \neq k}\left[\frac{3(\boldsymbol{\mu}_l \cdot \hat{\mathbf{r}}_{kl})\hat{\mathbf{r}}_{kl} - \boldsymbol{\mu}_l}{|r_{kl}|^3}\right],$$

(2)

where $\boldsymbol{\mu}_l = \sum_{i=1}^{n_{\text{atom}}} \mu_{\text{s}}^i \mathbf{S}_i$ is the magnetic moment of the micro-cell l containing n_{atom} spins. The thermal fluctuation of the spin moment site i arising from the effect of finite temperature is represented by the random field terms $\mathbf{B}_{\text{th}}^i$ in the following form:

$$\mathbf{B}_{\text{th},i} = \Gamma(t)\sqrt{\frac{2\alpha k_{\text{B}}T}{\gamma\mu_{\text{s}}\Delta t}},$$

(3)

where $\Gamma(t)$ is the thermal fluctuation represented by a Gaussian distribution.

The investigation of the magnetization reversal driven by spin-transfer torque can be achieved using the self-consistent solution of spin accumulation and spin current ($\mathbf{j}_m$), which is written as follows [31, 36–38]:

$$\mathbf{m}_\parallel (x) = \left[m_\parallel (\infty) + \left[m_\parallel (0) - m_\parallel (\infty) \right] e^{-x/\lambda_{sdl}} \right] \hat{\mathbf{b}}_1$$

$$\mathbf{m}_{\perp,2} (x) = 2e^{-k_1 x} \left[u \cos (k_2 x) - v \sin (k_2 x) \right] \hat{\mathbf{b}}_2$$

$$\mathbf{m}_{\perp,3} (x) = 2e^{-k_1 x} \left[u \sin (k_2 x) + v \cos (k_2 x) \right] \hat{\mathbf{b}}_3, \qquad (4)$$

where $\mathbf{m}_\parallel$ is the longitudinal component of spin accumulation, $\mathbf{m}_{\perp,2(3)}$ is the transverse component of spin accumulation, and the coefficients $(k_1 \pm i k_2) = \sqrt{\lambda_{sf}^{-2} \pm i \lambda_J^{-2}}$. $m_\parallel (\infty)$ denotes the spin accumulation at equilibrium, the spin-flip length is defined as $\lambda_{sf} = \sqrt{2 D_0 \tau_{sf}}$, and λ_J is the spin-precession length. The unknown variables u, v, and $m_\parallel (0)$ can be determined by considering the boundary conditions of the spin current across interfaces. The spin current at any position of the structure is written as follows:

$$\mathbf{j}_m (x) = \beta j_e \mathbf{M} - 2 D_0 \left[\frac{\partial \mathbf{m}}{\partial x} - \beta \beta' \mathbf{M} \left(\mathbf{M} \cdot \frac{\partial \mathbf{m}}{\partial x} \right) \right], \qquad (5)$$

where $\mathbf{M}$ is the unit vector of magnetization, β and β' are the spin polarization parameters of the material, j_e is the charge current density, and D_0 is the diffusion constant.

The MR ratio representing the performance of the read element is directly evaluated from the spatial spin accumulation and spin current described in the above equations. The microcell-based approach is applied to the system to determine the position dependence of the spin transport properties. The total RA of the system can be achieved by summing up the spatial (RA_i), which is expressed in terms of the gradient of spin accumulation (Δm) and spin current, given by

$$RA_{total} = \sum_{i=1}^{n} RA_i = \frac{V_{cell} k_B T}{e^2} \sum_{i=1}^{n} \frac{|\Delta m|}{|jm|} \qquad (6)$$

where n is the number of microcells, V_{cell} is the microcell volume, and e is the electron charge.

3. Results and discussion

To design a realistic CPP-GMR sensor, it is crucial to understand the mechanism of the EB phenomenon, which results from the coupling between AF and FM employed to set the magnetization direction of the PL, and which is responsible for the characteristics of the readback signal. Before considering the spin transport behavior in the reader stack, it is essential to verify the stability of the PL and the accuracy of the model by examining the magnetization dynamics of the layer. The investigation of EB can be initially studied by generating the bilayer system of AF/FM via the atomistic model implemented in the VAMPIRE software package [35]. A system of IrMn (6 nm)/CFS (4 nm) is considered to study the EB effect and to

Table 1. Magnetic and spin transport parameters of each material in the reader stack taken from [34–40].

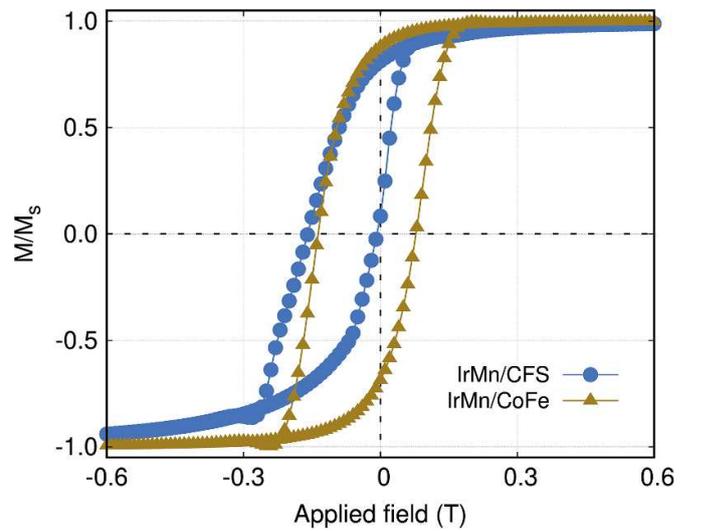| Parameter	IrMn	CFS	Ru	Ag	Unit
α	1.0	0.003			
T_c	690	1120			K
$k_u \times 10^{-24}$	422	0.28			J atom^{-1}
μ_s	2.50	5.54			μ_B
$J_{ij} \times 10^{-21}$	−6.4	4.89			J link^{-1}
β	0	0.86			
β'	0	0.96			
λ_{sdl}	0	1.7	600	160	nm
m_∞	0	15.71			MC m^{-3}
D_0	0	0.001	0.005	0.005	eV
$J_{IrMn-CFS}$	1.2×10^{-21}				J link^{-1}

Figure 1. The hysteresis loop of the bilayer system of IrMn (6 nm)/CFS (4 nm) and IrMn (6 nm)/CoFe (4 nm).

ensure that the magnetization of the PL is set before applying this system to the reader stack. The magnetic parameters of IrMn and CFS taken from previous studies are shown in table 1.

We simulate the hysteresis loop of CFS to calculate the EB field arising from the coupling with AF. As demonstrated in figure 1 (top), the hysteresis loop is shifted from the *y*-zero axis. The magnitude of the shifted loop defined as the EB field can be considered from the relation of the coercivity field (H_c), given by $H_{EB} = (H_c^- + H_c^+)/2$. The EB field for this system is approximately 81 mT, which is consistent with experiment [39]. The magnetization of CFS is fixed in the *x* direction corresponding to the EB field. Furthermore, we also make a comparison of the EB field occurring in the system of IrMn (6 nm)/CoFe (4 nm) where the EB field is 50 mT. This demonstrates that utilizing CFS as the PL results in a higher EB field and a more stable PL. For the rest of the investigations in this paper, CFS Heusler alloy is therefore designated to serve as the PL, reference layer, and FL in the reader stack.
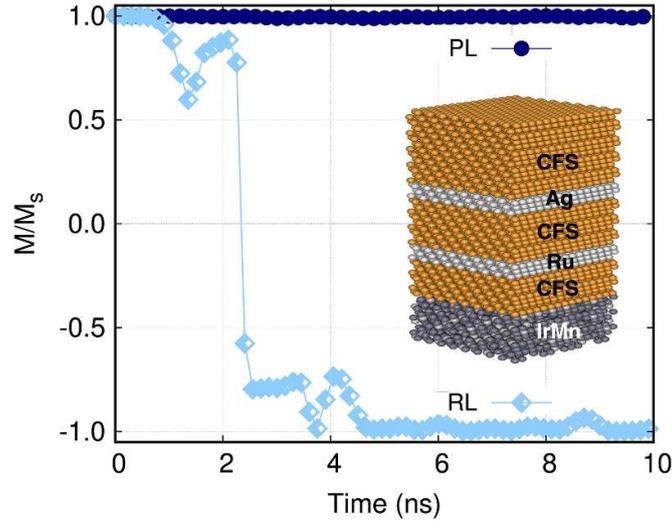
J. Phys. D: Appl. Phys. **57** (2024) 135001

R Khamtawi *et al*

Figure 2. The time evolution of the *x* component of magnetization in PL and RL in the reader stack of IrMn/CFS/Ru/CFS/Ag/CFS.

Next, a simple reader stack of IrMn/CFS/Ag/CFS is constructed using an atomistic model to check the direction of magnetization of each layer before introducing the spin current into the system and investigating the spin transport behavior in the reader stack. It is necessary to check the magnetization dynamics of the PL to confirm its stability and the validity of the model. After performing EB simulation to obtain the direction of the PL, we then construct the whole reader stack by putting the IrMn/CFS together with the Ag/CFS system. The time evolution of the magnetization can be observed by the atomistic model via the LLG equation. Furthermore, as demonstrated in figure 2, the SAF structure, which provides the reference direction in the magnetoresistive sensors, is taken into consideration for the realistic reader model of IrMn/CFS/Ru/CFS/Ag/CFS since the performance and magnetic stability of the device can be improved by inserting the SAF layer. The effect of the diffused interfaces is also included in the system. The results in figure 2 obtained from the atomistic simulations show the *x* component of magnetization in the PL and reference layer, which are oriented in the opposite direction due to the indirect exchange coupling between these two layers, known as the Rudermann–Kittel–Kasuya–Yosida (RKKY) exchange interaction. In addition, the SAF layer reduces the effect of the stray field from the PL acting on the magnetization of the FL, resulting in a more stable magnetization of the FL aligned in the easy axis direction. The correctness of the model can be confirmed by the direction of magnetization of both layers before investigating the spin transport within the magnetic structure.

The spin transport behavior in the reader stack with and without the SAF layer is studied for both the parallel (P) and anti-parallel (AP) states, where the relative magnetization is aligned in the same direction and opposite direction, respectively. A charge current with a density of $1\,\mathrm{MA\,cm^{-2}}$ is injected into the system. The results show that the spin accumulation and spin current tend to align in the direction of local

magnetization, and a large change in spin accumulation can be observed in the region of the diffuse interface between layers due to the difference in spin transport properties as shown in figure 3. For the P state, the spin-polarized current can easily flow through the magnetic structure, yielding low resistance in both systems, with and without the SAF layer. The value of the RA product of the AP state is higher than that of the P state, as expected. Subsequently, the MR ratio of both systems can be evaluated. Importantly, the reader stack with the SAF layer provides a high RA of $30.22\,\mathrm{m\Omega\cdot\mu m^2}$ and enhances the MR ratio up to 73.24% at 0 K, which is in excellent agreement with previous experiments [40, 41], whereas the reader stack without the SAF layer gives a lower RA of $16.75\,\mathrm{m\Omega\cdot\mu m^2}$ and a low MR ratio of 16.79%. This may be explained by the fact that the number of interfaces has a significant impact on the RA and MR ratio values, which are strongly contingent on both bulk and interfacial spin scatterings. The significant difference in MR ratio between the systems with and without the SAF layer indicates the importance and requirement of the realistic reader model to predict and design the read head of HDDs.

Subsequently, the effect of current density on the performance of the reader stack including the SAF structure is considered by varying the current density from $1\,\mathrm{MA\,cm^{-2}}$ to $5\,\mathrm{MA\,cm^{-2}}$. With the aid of this investigation, we are able to determine the optimal current density for reading HDDs with a recording density beyond $2\,\mathrm{Tbit\,in^{-2}}$. An increase in the current density enhances the efficiency of spin transport, and a high-spin polarized current can flow into the reader stack. The Heusler-alloy-based read sensor gives a low RA of less than $\mathrm{RA} < 100\,\mathrm{m\Omega\cdot\mu m^2}$ and a high MR ratio of up to 120%, as shown in figure 4, which is consistent with the experimental results in [42]. The results demonstrate a better performance of the read sensor with Heusler alloy than that with conventional FMs, such as CoFe and NiFe [23, 43, 44]. Previously, Heusler alloy material has been utilized as the FL in the read
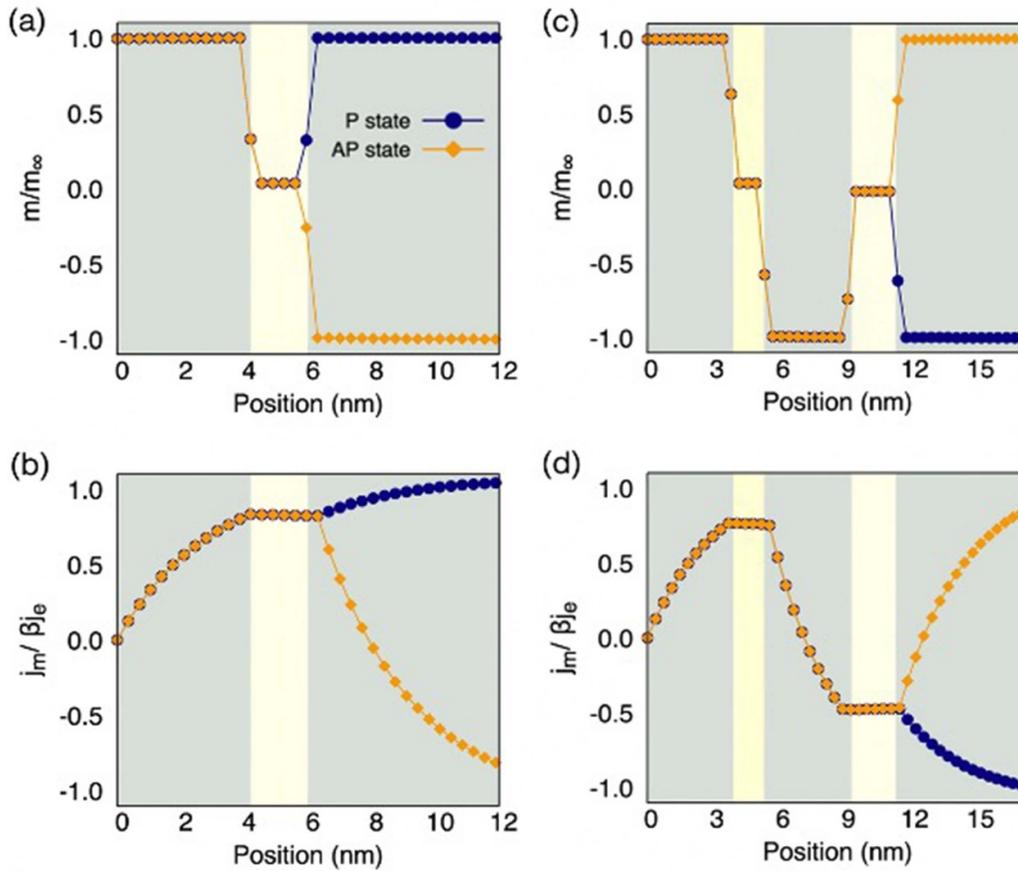
Figure 3. (a) The spatial variation of spin accumulation and (b) spin current within the conventional reader stack of IrMn/CFS/Ag/CFS; (c) the spin accumulation and (d) the spin current within the full reader stack of IrMn/CFS/Ru/CFS/Ag/CFS after introducing the charge current density of $1\,MA\,cm^{-2}$.

element, giving a low RA of less than $100\,m\Omega \cdot \mu m^2$ and a high MR ratio [45, 46]. In this work, it is applied in the reader stack to serve not only as the PL but also as the reference layer and FL. The spin-polarized current easily flows into the structure. As a result, a higher MR ratio and lower $RA < 40\,m\Omega \cdot \mu m^2$ are observed, which aligns with the criteria for ultra-high-capacity HDDs as well as being consistent with previous studies [40, 43, 47].

As illustrated in figure 4 (top), the spin transport behavior in the full reader stack of IrMn/CFS/Ru/CFS/Ag/CFS can be explained in two regions. For the region of low current density, $j_e < 2\,MA\,cm^{-2}$, increasing the charge current density slightly decreases the value of RA in both the P and AP states, and this consequently yields a small change in the MR ratio, which is approximately 73.24%. Although the small charge current density provides a high MR ratio, the average RA value

calculated from the RA of the P and AP states is still high. The rapid change of RA is noticeable at the current density of $2\,MA\,cm^{-2}$. At high current density in the region of $j_e > 2\,MA\,cm^{-2}$, the RA of both the P and AP states is relatively little altered after the abrupt decrease. The MR ratio gradually increases and reaches saturation at high current densities. It is suggested that the optimal current density to obtain a high MR ratio and low RA is approximately $3\,MA\,cm^{-2}$. Furthermore, the capacity of HDDs or the AD, which is inversely proportional to the RA, is calculated next. Figure 4 (bottom) shows the AD as a function of the RA. According to the results, the Heusler alloy read elements with $RA < 10\,m\Omega \cdot \mu m^2$ can be applied to future HDDs with an AD greater than $2\,Tbit\,in^{-2}$. The possibility for a wide variety of Heusler alloy materials in device applications is demonstrated by these investigations.
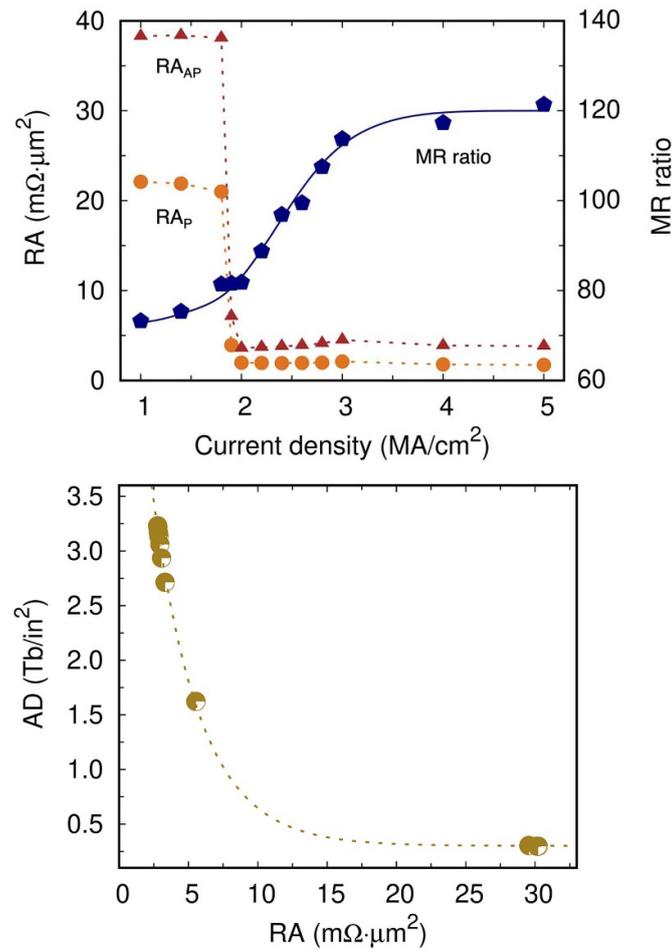
Figure 4. (Top) The variation of RA product and MR ratio as a function of injected current density; (bottom) the relationship between RA and the areal density of the IrMn/CFS/Ru/CFS/Ag/CFS structure.

4. Conclusions

The Heusler alloy-based CPP-GMR sensor is studied in this work as an alternative choice to support future HDDs with ultra-high recording densities. To design a realistic read element, the full stack of the reader, including the EB phenomenon and SAF layer, is taken into consideration. The atomistic model is used to construct the reader stack and investigate the magnetization dynamics. The spin accumulation model is employed to evaluate the spin transport behavior in the reader stack. This theoretical investigation shows that the systems with and without SAF produce different results. The reader stack with the SAF layer provides a high RA of $30.22 \, \mathrm{m\Omega \cdot \mu m^2}$ and enhances the MR ratio up to 73.24% at 0 K, which is consistent with prior studies. Therefore, the inclusion of the SAF layer becomes crucial for accurate modeling. Next, the Heusler alloy was utilized in a reader stack of IrMn/CFS/Ru/CFS/Ag/CFS. It was found that a low current density of $3 \, \mathrm{MA \, cm^{-2}}$ can be applied to the structure to achieve a high MR ratio, low RA, and AD of over $2 \, \mathrm{Tbit \, in^{-2}}$.

Data availability statement

The data that support the findings of this study are available upon reasonable request from the authors.

Acknowledgments

ORCID iDs

J Chureemart ⓘ https://orcid.org/0000-0002-1318-9266
P Chureemart ⓘ https://orcid.org/0000-0002-1199-7809

J. Phys. D: Appl. Phys. **57** (2024) 135001

R Khamtawi *et al*

References

[1] Pinarbasi M and Kent A D 2022 *APL Mater.* **10** 020901
[2] Albuquerque G, Hernandez S, Kief M T, Mauri D and Wang L 2022 *IEEE Trans. Magn.* **58** 1
[3] Chen Y *et al* 2010 *IEEE Trans. Magn.* **46** 697
[4] Wood R 2009 *J. Magn. Magn. Mater.* **321** 555
[5] Nakatani T, Gao Z and Hono K 2018 *MRS Bull.* **43** 106–11
[6] Wang J-H, Choong W-K, Chen C-T and Sung T-Y 2022 *Sci. Rep.* **12** 2045
[7] Mao S *et al* 2006 *IEEE Trans. Magn.* **42** 97
[8] Yan S, Zhou Z, Yang Y, Leng Q and Zhao W 2022 *Tsinghua Sci. Technol.* **27** 443
[9] Liu E *et al* 2018 *Phys. Rev. Appl.* **10** 054054
[10] Diao Z *et al* 2014 *J. Magn. Magn. Mater.* **356** 73
[11] Inomata K, Tezuka N, Okamura S, Kurebayashi H and Hirohata A 2004 *J. Appl. Phys.* **95** 7234
[12] Atsufumi Hirohata A, Sagar J, Lari L, Fleet L R and Lazarov V K 2013 *Appl. Phys.* A **111** 423–30
[13] Elphick K, Frost W, Samiepour M, Kubota T, Takanashi K, Sukegawa H, Mitani S and Hirohata A 2021 *Sci. Technol. Adv. Mater.* **22** 235
[14] Hirohata A *et al* 2006 *Curr. Opin. Solid State Mater. Sci.* **10** 93
[15] Hirohata A, Sukegawa H, Yanagihara H, Zutic I, Seki T, Mizukami S and Swaminathan R 2015 *IEEE Trans. Magn.* **51** 1
[16] Chatterjee S, Samanta S, Ghosh B and Mandal K 2023 *Phys. Rev.* B **108** 205108
[17] Nakatani T M *et al* 2012 *IEEE Trans. Magn.* **48** 1751
[18] Bombor D, Blum C G F, Volkonskiy O, Rodan S, Wurmehl S, Hess C and Büchner B 2013 *Phys. Rev. Lett.* **110** 066601
[19] Kuerbanjiang B *et al* 2016 *Appl. Phys. Lett.* **108** 172412
[20] Chen P J, Feng G and Shull R D 2013 *IEEE Trans. Magn.* **49** 4379
[21] Kabanov Y P, Shull R D, Zheng C, Pong P W T, Gopman D B and Shashkov I V 2022 *J. Surf. Invest.: X-ray Synchrotron Neutron Tech.* **16** 201–6
[22] Mahat R, Karki U, KC S, Law J Y, Franco V, Galanakis I, Gupta A and LeClair P 2022 *Phys. Rev. Mater.* **6** 064413
[23] Saenphum N, Chureemart J, Evans R F L, Chantrell R W and Chureemart P 2021 *J. Phys. D: Appl. Phys.* **54** 395004
[24] Aoshima K, Funabashi N, Machida K, Miyamoto Y, Kuga K and Kawamura N 2007 *J. Magn. Magn. Mater.* **310** 2018
[25] Dubowik J, Gościańska I, Załęski K, Głowiński H, Kudryavtsev Y and Ehresmann A 2013 *J. Appl. Phys.* **113** 193907
[26] Raza S, Correa M, Gonzalez-Chavez D, Bohn F and Sommer R 2021 *Mater. Lett.* **291** 129518
[27] Jana A, Raja M, Chelvane J, Ghosal D P and Jammalamadaka S 2022 *J. Supercond. Novel Magn.* **35** 1313–9
[28] Jiang Y, Abe S, Ochiai T, Nozaki T, Hirohata A, Tezuka N and Inomata K 2004 *Phys. Rev. Lett.* **92** 167204
[29] Leal J L and Kryder M H 1998 *J. Appl. Phys.* **83** 3720
[30] Sharma P P, Albisetti E, Monticelli M, Bertacco R and Petti D 2016 *Sensors* **16** 1030
[31] Saenphum N, Chureemart J, Chantrell R and Chureemart P 2019 *J. Magn. Magn. Mater.* **484** 238
[32] Meo A, Chureemart J, Chantrell R W and Chureemart P 2022 *Sci. Rep.* **12** 3380
[33] Sanvito S, Lambert C J and Jefferson J H 2000 *Phys. Rev.* B **61** 14225
[34] Chureemart P, Evans R F L, D'Amico I and Chantrell R W 2015 *Phys. Rev.* B **92** 054434
[35] Evans R F L *et al* 2014 *J. Phys.: Condens. Matter* **26** 103202
[36] Chureemart P, Cuadrado R, D'Amico I and Chantrell R W 2013 *Phys. Rev.* B **87** 195310
[37] Chureemart P, D'Amico I and Chantrell R W 2015 *J. Phys.: Condens. Matter* **27** 146004
[38] Chureemart J, Cuadrado R, Chureemart P and Chantrell R 2017 *J. Magn. Magn. Mater.* **443** 287
[39] Childress J R, Schwickert M M, Fontana R E, Ho M K, Rice P M and Gurney B A 2001 *J. Appl. Phys.* **89** 7353
[40] Nakatani T M, Furubayashi T and Hono K 2011 *J. Appl. Phys.* **109** 07B724
[41] Furubayashi T, Nakatani T M, Goripati H S, Sukegawa H, Takahashi Y K, Inomata K and Hono K 2013 *J. Appl. Phys.* **114** 123910
[42] Sakuraba Y, Ueda M, Miura Y, Sato K, Bosu S, Saito K, Shirai M, Konno T J and Takanashi K 2012 *Appl. Phys. Lett.* **101** 252408
[43] Hirohata A *et al* 2020 *J. Magn. Magn. Mater.* **509** 166711
[44] Deak J G, Zhou Z and Shen W 2017 *AIP Adv.* **7** 056676
[45] Kubota T, Wen Z and Takanashi K 2019 *J. Magn. Magn. Mater.* **492** 165667
[46] Kabanov Y P, Shull R D, Zheng C, Pong P W T and Gopman D B 2021 *Appl. Surf. Sci.* **536** 147672
[47] Chen J *et al* 2020 *Acta Mater.* **200** 1038